Mode analysis and signal restoration with Kravchuk functions

Kurt Bernardo Wolf

Instituto de Ciencias Físicas, Universidad Nacional Autónoma de México, Av. Universidad s/n, Cuernavaca, Morelos 62251, Mexico (bwolf@fis.unam.mx)

Received August 28, 2008; accepted December 8, 2008; posted December 23, 2008 (Doc. ID 100739); published February 12, 2009

When a continuous-signal field is sampled at a finite number N of equidistant sensor points, the N resulting data values can yield information on at most N oscillator mode components, whose coefficients should in turn restore the sampled signal. We compare the fidelity of the mode analysis and synthesis in the orthonormal basis of N-point Kravchuk functions with those in the basis of sampled Hermite–Gauss functions. The scale between the two bases is calibrated on the ground state of the field. We conclude that mode analysis is better approximated in the nonorthogonal sampled Hermite–Gauss basis, while signal restoration in the Kravchuk basis is exact. © 2009 Optical Society of America

OCIS codes: 070.2025, 070.4790.

1. INTRODUCTION

Assume that in a planar acoustical or optical multimodal waveguide, the field across the guide is recorded by sampling the continuous complex function $F(x)$ on $N=2j+1$ equally spaced "sensor" points $x_m=sm$, for integer or half-integer $m|_{-j}^{j}$, and an appropriate scale factor s to be determined. From this collection of N complex data values, the signal $\{F(m)\}_{m=-j}^{j}$, we should (approximately) find the first N formant harmonic oscillator mode coefficients of the continuous field, and from these, if possible, restore the original sampled signal.

In the continuum, the harmonic oscillator modes are the well-known Hermite–Gauss (HG) functions $\{\Psi_n(x)\}_{n=0}^{\infty}$, which form a complete and denumerable orthonormal basis for the Hilbert space of square-integrable functions $\mathcal{L}^2(\Re)$ under its standard scalar product that integrates over $x|_{-\infty}^{\infty}$. On the other hand, under the usual scalar product of N-dimensional complex vector spaces $\mathcal{V}^N$, the corresponding N sampled-HG (s-HG) N-vectors $\{\Psi_n(x_m)\}_{n=0}^{N-1}$ (with components numbered by $m|_{-j}^{j}$), are linearly independent—but not orthogonal. There is ample literature on the analysis of signals by HG functions [1–5] that discusses their remarkable properties under the Fourier transform [6,7]. For $\mathcal{V}^N$ we have also the orthonormal basis of discrete Kravchuk functions $\{\Phi_n^j(m)\}_{n=0}^{N-1}$, which derive from oscillator dynamics [8–10]. The aim of this paper is to elucidate the relative advantages of each of these two bases for the two tasks we set forth above: namely, analyzing the mode content and synthesizing back the signal.

At the outset we must indulge in the abstraction that the field can be subject to measurement at a point—actual sensors have finite size of course; and while the measurement of amplitude and phase is possible in acoustics, optical arrangements will require extra provisions. We note that since in a waveguide neither the continuous field nor the finite signal is actually periodic modulo N, the free waves of Fourier analysis would not provide the best basis for this analysis in $\mathcal{V}^N$. Thus, we recall in Section 2 the s-HG and Kravchuk bases. In finite systems, the sampled data "exist" only on the N sensor points (numbered by $m|_{-j}^{j}$); yet both the s-HG and the Kravchuk functions are analytic on the complex m plane; for mathematical instruction we shall keep track of the behavior of signals on the real interval $m\in[-j,j]$.

The context of this work is the approximation of finite to continuous models of optics, one of whose aspects is finding the optimal free parameters to center and scale the sensor array [11]. In Section 3 our approach calibrates the optimal scale between the s-HG and Kravchuk functions with the ground state of the field. The validity of this choice comes to the fore in Section 4, bringing up the nonorthogonality of the s-HG basis versus the orthonormal Kravchuk basis as we analyze and synthesize signals. In fact, the s-HG basis is better used with a different analysis, which is applied in Section 5 to compare the s-HG and Kravchuk syntheses of a rectangle signal. The "discontinuities" of the rectangle emphasize the Gibbs-like oscillations that impede the exact restoration of the signal. In Section 6 we offer some conclusions and suggest straightforward extensions for two-dimensional sensor configurations.

2. SAMPLED-HG AND KRAVCHUK BASES

The natural structure for finitely sampled N-point signals, $\{F(m)\}$, $\{G(m)\}$, is that of a complex vector space $\mathcal{V}^N$, characterized by its scalar product,

$$(F,G)_N := \sum_{m=-j}^{j} F(m)^* G(m), \tag{1}$$

where $N=2j+1$ and * means complex conjugation. The norm of a signal is $|F| := \sqrt{(F,F)}$, and the angle between the two is $\cos\theta_{F,G} := (F,G)_N/|F||G|$. We consider two vector bases for $\mathcal{V}^N$ that approximate the continuous-oscillator dynamics: sampled HG and Kravchuk functions.

The normalized s-HG function basis is the set of real vectors in $\mathcal{V}^N$ sampled from the continuous oscillator functions,

$$\Psi_n^{(s)}(m) := A_n(s)\exp\left(-\tfrac{1}{2}s^2m^2\right)H_n(sm), \qquad n|_0^{N-1}, \quad (2)$$

where $A_n(s)$ is the factor that sets $|\Psi_n^{(s)}|=1$. The continuous-oscillator Hamiltonian $\frac{1}{2}(-\nabla^2+x^2)$ is approximated in $\mathcal{V}^N$ by the $N\times N$ matrix whose eigenvectors are Eq. (2) with eigenvalues $n+\frac{1}{2}$. To find this matrix one needs to compute the dual basis since, except for parity, two s-HG vectors are not orthogonal. The exponential of this matrix builds a one-parameter cyclic subgroup of matrices that is the fractional Fourier transform associated with the s-HG basis [12]. This imposes harmonic motion on the vectors of this basis.

The Kravchuk functions stem from the harmonic motion provided by the rotation (spin) group SU(2), well known from quantum angular momentum theory [13], which has matrix representations of dimensions $N=2j+1$, for j a positive integer or half-integer. In this SU(2) oscillator model [8], the position, momentum, and (displaced) energy observables are identified with the eigenvalues of the generators of rotations around the 1-, 2-, and 3-axis, respectively; for each j, all have thus intrinsically the same discrete, finite spectrum $m|_{-j}^{j}$. The Kravchuk functions $\Phi_n^j(m)$ of mode number $n|_0^{2j}$ and position $m|_{-j}^{j}$ are the overlaps between the eigenvectors of the Hamiltonian generator of rotations around the 3-axis and the eigenvectors of the position operator, which is the generator of rotations around the 1-axis. These overlaps are the well-known SU(2) Wigner "little-d" functions for the angle $\frac{1}{2}\pi$, which can be expressed as the product of the square root of a binomial times a symmetric Kravchuk polynomial [14] as [8]

$$\Phi_n^j(m) := d^j_{n-j,m}\left(\tfrac{1}{2}\pi\right) = \frac{(-1)^n}{2^j}\sqrt{\binom{2j}{n}\binom{2j}{j+m}}K_n\left(j+m;\tfrac{1}{2},2j\right), \quad (3)$$

$$K_n\left(j+m;\tfrac{1}{2},2j\right) = {}_2F_1(-n,-2j-m;-2j;2) = K_{j+m}\left(n;\tfrac{1}{2},2j\right), \quad (4)$$

and have the symmetry properties

$$\Phi_n^j(m) = (-1)^n\Phi_n^j(-m) = (-1)^{n-j}\Phi_{2j-n}^j(m) = (-1)^{n-j-m}\Phi_{j+m}^j(n-j). \quad (5)$$

When N is even, j and m are half-integers; although the formalism applies straightforwardly, there is an extra sign for global transformations owing to the 2:1 cover of the unitary group SU(2) over the rotation group SO(3). To avoid this possible complication—and to have a sensor point at $m=0$—we shall consider here only odd numbers N of points, so j and m will be integers. Finally, in the $N\to\infty$ limit, Kravchuk functions converge pointwise to the continuous-oscillator functions on the full finite line [15],

$$\lim_{j\to\infty}(-1)^{n+j}j^{1/4}\Phi_n^j(m) = \Psi_n(x) \qquad \text{for } x=m/\sqrt{j}. \quad (6)$$

The chosen SU(2) group generators are self-adjoint, so the Kravchuk basis (3) is orthogonal, and it has been chosen orthonormal: $(\Phi_n^j,\Phi_{n'}^j)_N=\delta_{n,n'}$. Note in Eq. (3) that since $K_n(j+m;\cdot,\cdot)$ is a polynomial of degree n in m, and also the binomial coefficient $\binom{2j}{j+m}$ has a unique analytic continuation, the Kravchuk functions are analytic in the complex-m plane; they have branch-point zeros at $m=\pm(j+k)$ for integer $k\geqslant 1$ (so there is "nothing" beyond the signal end points). In Fig. 1 we show the Kravchuk functions $\Phi_n^j(m)$ for discrete $m\in[-j,j]$, analytically continued in that interval, and the corresponding s-HG functions $\Psi_n^{(\bar{s})}(m)$ with a scale $\bar{s}$ that is optimized to match the ground states, to be determined next.

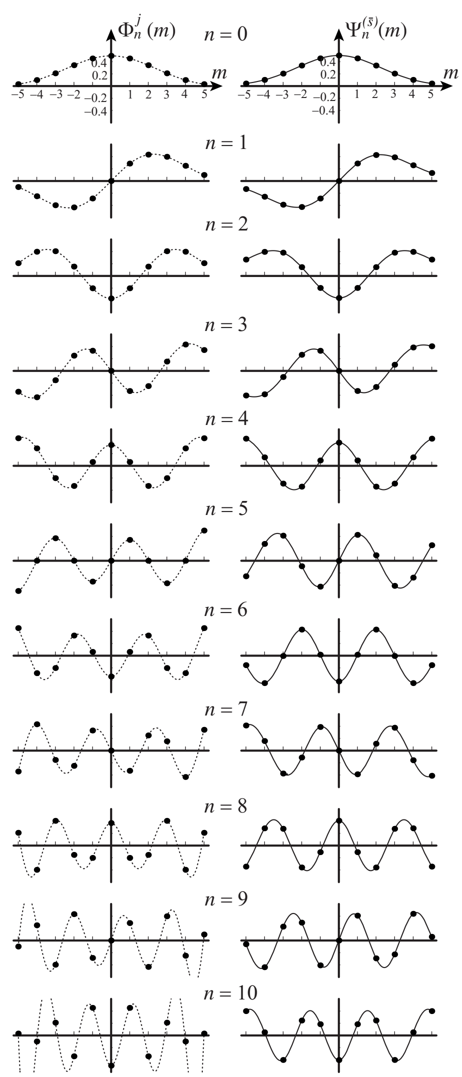

Fig. 1. Left column, Kravchuk basis functions, $\Phi_n^j(m)$ in Eq. (3), for $j=5$ (marked with dots on the $N=11$ points); dotted curves show their analytic continuation to $m\in[-5,5]$. Right column, s-HG functions $\Psi_n^{(\bar{s})}(m)$ in Eq. (2); dots indicate the sampling points for an optimal scale factor $\bar{s}=0.446410$. From top to bottom are the vectors of 11 basis states $n|_0^{10}$. Note that as a result of Eq. (5), the higher Kravchuk modes $6\leqslant n\leqslant 10$ have the same absolute values as the lower modes $0\leqslant n\leqslant 4$.

3. CALIBRATION OF SCALE

We propose that the sensor array that samples the field and yields the signal can be calibrated so that the ground HG beam is centered and so that its sampling $\Psi_0^{(s)}(m)$ results in an optimal match with the ground Kravchuk vector $\Phi_0^j(m)$. This is the square root of a binomial distribution,

$$\Phi_0^j(m) = \frac{1}{2^j}\sqrt{\binom{2j}{j+m}}, \qquad m|_{-j}^{j}. \tag{7}$$

In Fig. 2 we compare Eq. (7) with the normalized s-HG ground state for various scale factors s around an optimal value $\bar{s}$ where the two are visually indistinguishable.

The question naturally arises how appropriate is this "optimal" scale for all other modes. The relation between the Kravchuk and s-HG basis vectors with scale s is contained in a set of N difference N-vectors,

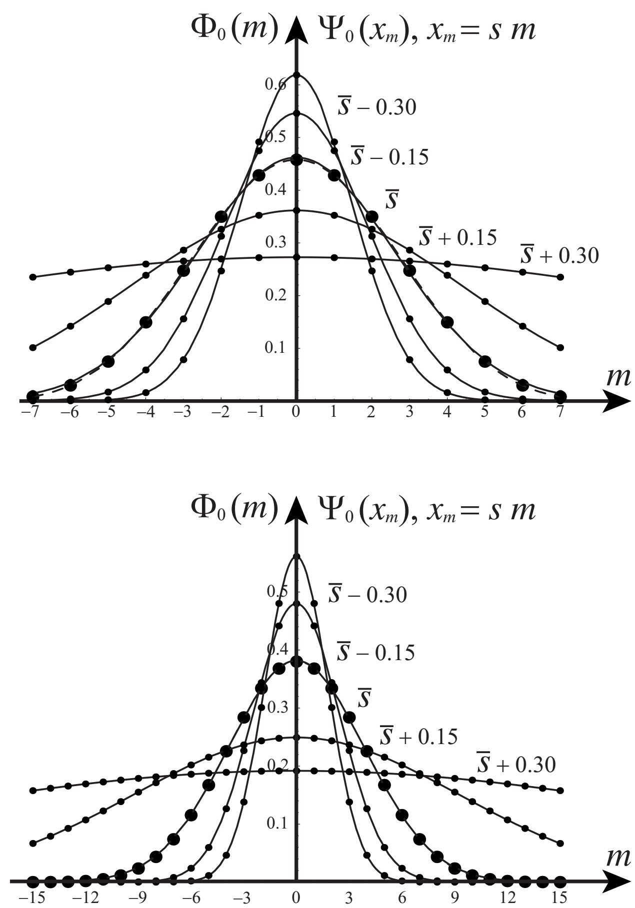

Fig. 2. Scale calibration of the ground s-HG vector to the ground Kravchuk vector. Top, for $j=7$ ($N=15$ points); bottom, for $j=15$ ($N=31$ points). Large dots mark the values of the Kravchuk function $\Phi_0^j(m)$. Solid curves show the s-HG function $\Psi_0(x_m)$; Small-dots mark the sampling points $x_m=sm$, for scale factors s around the optimal value $\bar{s}$ where the s-HG and Kravchuk functions are closest. For $j=7$, this is $\bar{s}=0.378138$, and for $j=15$ it is $\bar{s}=0.258253$. The dashed curve (barely visible in the top figure near the center and edges of the interval) is the analytic continuation of the ground Kravchuk function.

$$D_n^{(s)}(m) := \Psi_n^j(m) - \Psi_n^{(s)}(m), \qquad n|_0^{2j}. \tag{8}$$

None of these vectors can be zero for any scale s, but for each $n|_0^{N-1}$ one can find values $\bar{s}_n^j$ that minimize the norm of the difference vectors,

$$D_n^j := \min_s |D_n^{(s)}| = |D_n^{(\bar{s})}|. \tag{9}$$

The vectors in both bases are normalized so the angle between each pair of corresponding modes n, $\theta_n^j(s) := \arccos(\Phi_n^j, \Psi_n^{(s)})_N$, is also minimized for $s=\bar{s}_n^j$.

In Fig. 3 we show the difference norms $|D_n^{(s)}|$ for all modes and a range of scale factors. There is a single minimum for the ground state, $\bar{s}_0^j$, because both functions have single positive and centered bulges; we see that this minimum has a clear continuation into the higher-n region, where several minima can occur when the quasi-period of the s-HG functions comes close to a multiple or submultiple of the sign alternation period in the Kravchuk functions. For concreteness, we tabulate the following low-n scale factors, difference norms, and angles (in degrees) between the s-HG and Kravchuk basis vectors, indicating

$$\bar{s}_n^j, \quad \text{best value of the scale } s,$$

$$|D_n^{(\bar{s})}|, \quad \text{norm of difference vector at } \bar{s}_n^j,$$

$$\theta_n^j, \quad \text{angle between the vectors at } \bar{s}_n^j. \tag{10}$$

For first few models $n|_0^5$ and for arrays between 11 and 31 sensors, these are as follows:

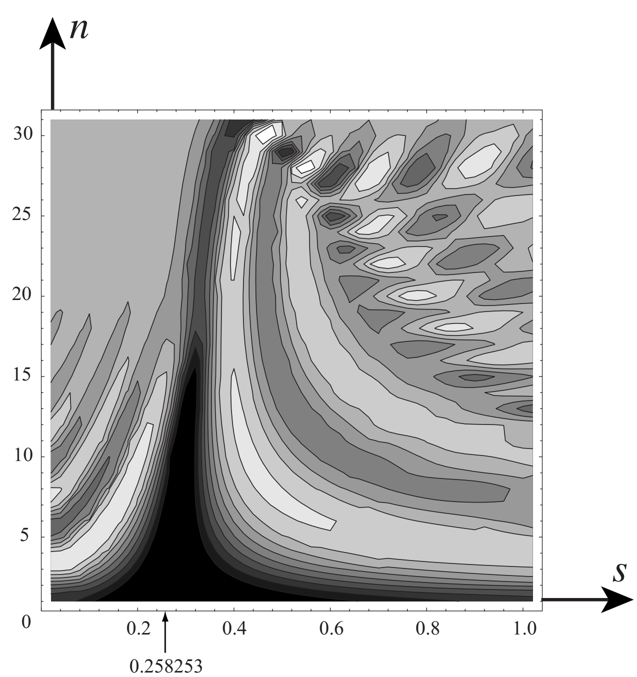

Fig. 3. Density plot of the norm of the difference vector $|D_n^{(s)}|$ in Eq. (9) for $j=15$ ($N=31$ points), over the ranges $n|_0^{30}$ and $0<s<1$. We adopt the optimum value at the $n=0$ ground state, $\bar{s}^j=0.258253$.

$j(N)$	5(11)	7(15)	9(19)	11(23)	13(27)	15(31)
	0.446410	**0.378138**	**0.333515**	**0.301632**	**0.277429**	**0.258253**
$n=0$:	0.019418	0.015702	0.012382	0.010027	0.008383	0.007196
	1.113°	0.899°	0.709°	0.574°	0.480°	0.412°
	0.459067	**0.387106**	**0.339919**	**0.306390**	**0.281117**	**0.261214**
$n=1$:	0.038087	0.034659	0.028435	0.023206	0.019358	0.016547
	2.182°	1.986°	1.629°	1.330°	1.109°	0.948°
	0.465404	**0.393058**	**0.344594**	**0.309960**	**0.283890**	**0.263430**
$n=2$:	0.061012	0.064049	0.055706	0.046456	0.038952	0.033283
	3.496°	3.670°	3.192°	2.662°	2.232°	1.907°
	0.472270	**0.399089**	**0.349729**	**0.314058**	**0.287129**	**0.266030**
$n=3$:	0.061512	0.087453	0.084336	0.073291	0.062266	0.053278
	3.525°	5.012°	4.834°	4.200°	3.569°	3.053°
	0.484325	**0.405105**	**0.354900**	**0.318405**	**0.290666**	**0.268900**
$n=4$:	0.062078	0.097435	0.109893	0.102186	0.089274	0.077050
	3.557°	5.585°	6.300°	5.857°	5.117°	4.416°
	0.504866	**0.412380**	**0.359923**	**0.322743**	**0.294333**	**0.271938**
$n=5$:	0.137602	0.098467	0.127387	0.130108	0.118937	0.104628
	7.890°	5.644°	7.304°	7.460°	6.819°	5.998°

. (11)

As expected, we see that the alignment between the vectors in the two bases improves with growing number of points (to the right) and worsens with increasing mode number n, down. Our working proposition is that the optimal scale for $n=0$, $\bar{s} := \bar{s}_0^j$, will serve best for all signals.

4. EXPANSION IN KRAVCHUK AND s-HG MODES

The basis of N Kravchuk vectors $\{\Phi_n^j\}_{n=0}^{2j}$ in Eq. (3) is orthonormal and complete in $\mathcal{V}^N$. Its vectors provide a comfortable basis for the vector space, and every N-point signal $\{F(m)\}_{m=-j}^{j}$ can be synthesized and analyzed through

$$F(m) = \sum_{n=0}^{2j} F_n^{\mathrm{K}} K_{n,m}^j, \qquad F_n^{\mathrm{K}} = \sum_{m=-j}^{j} K_{n,m}^j F(m),$$

$$K_{n,m}^j := \Phi_n^j(m), \tag{12}$$

where the N-vector of Kravchuk mode coefficents is $\{F_n^{\mathrm{K}}\}_{n=0}^{2j}$. The Kravchuk transform matrix $K_{n,m}^j = \Phi_n^j(m)$ is shown as a density plot in Fig. 4 (adapted from Fig. 7 of [12]); since it is unitary and real (thus orthogonal), $(K^j)^{-1}$ is the transpose of K^j (with $m \leftrightarrow n+j$), $\det K^j = 1$, and the Parseval identity implies that $|F^{\mathrm{K}}| = |F|$.

When we apply the same straightforward analysis to the set of N optimally scaled and normalized s-HG vectors $\{\Psi_n^{(\bar{s})}(m)\}_{m=-j}^{j}$ in Eq. (2), since they are not orthogonal we have to invert the matrix of vectors to find its dual basis,

$$F(m) = \sum_{n=0}^{2j} F_n^{\mathrm{S}} S_{n,m}, \qquad F_n^{\mathrm{S}} = \sum_{m=-j}^{j} (S^{-1})_{n,m} F(m),$$

$$S_{n,m} := \Psi_n^{(\bar{s})}(m). \tag{13}$$

The determinant of the transform matrix S would be zero, and the s-HG basis incomplete, if two or more vectors in

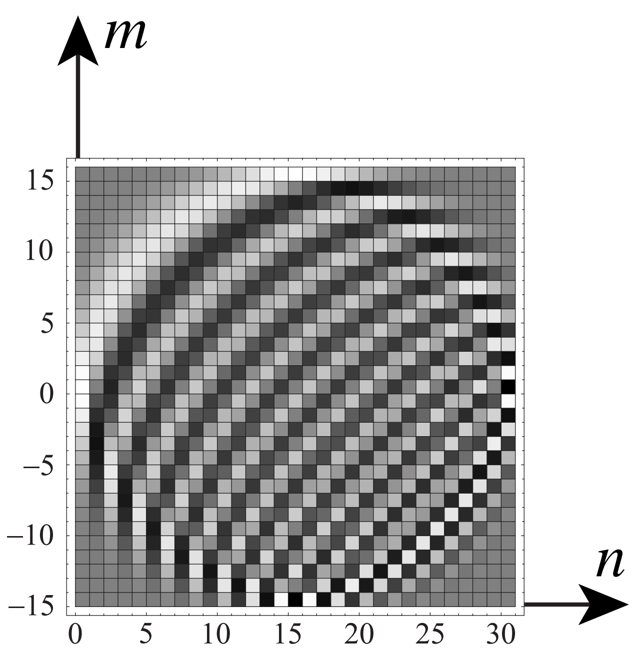

Fig. 4. Density plot for the elements of the 31×31 unitary Kravchuk transform matrix $K_{n,m}^j = \Phi_n^j(m)$ in Eq. (3) for $j=15$. Each column represents one Kravchuk vector $n|_0^{30}$; gray is zero; light and dark pixels correspond to positive and negative values. Owing to the symmetry properties (5), the left half of the figure reflects the right half with a sign alternation. (Adapted from Fig. 7 of [12]).

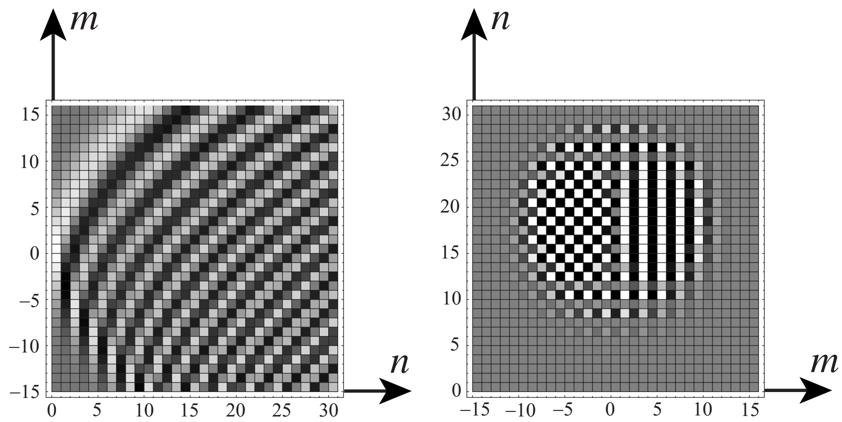

Fig. 5. Left, density plot for the elements of the s-HG matrix $S_{n,m} := \Psi_n^{(\bar{s})}(m)$ in Eq. (13); as in Fig. 4, each column represents a sampled HG mode. Here $j=15$, $m|_{-15}^{15}$, $n|_0^{30}$, and $\det S = 2.33458 \times 10^{-41}$; the maximum element of S is $S_{0,0}=0.3817$. Right, the dual basis given by the elements of the inverse matrix $(S^{-1})_{n,m}$; the maximum elements are $S^{-1}_{19,\pm 1} = 6.054 \times 10^7$. (Adapted from Fig. 1 of [12]).

the set were linearly dependent. Actually, the s-HG basis is "barely" complete for $\mathcal{V}^N$: in the case $N=31$ ($j=15$), its determinant is $\det S = 2.33 \times 10^{-41}$. This does not seem to be a numerical obstacle to computing the coefficients: the elements of $S^{-1}S$ were found to differ from the unit matrix by less than 10^{-7}. The real problem with using this basis is illustrated by Fig. 5, where we show the s-HG vectors of the matrix S (adapted from Fig. 1 of [12]), and their dual basis in S^{-1}, also by density plots as for the Kravchuk basis in Fig. 4. This dual basis is rather surprising because it indicates that in mode analysis, when this matrix acts on the column vector of signal values $F(m)$, the higher mode coefficients (roughly $8 < n < 28$) will be greatly enhanced over all lower ones, inordinately punching out these coefficients.

To play fairly however, the basis of s-HG vectors $\{\Psi_n^{(\bar{s})}\}_{n=0}^{2j}$ can be used in a much better way to analyze the modes of the N-point signal $F(m)$ by succesively projecting out, from $n=0$ up, the components of the signal along each basis vector. This leads to a recursive algorithm for the sequence of difference vectors:

$$\Delta^{(n+1)}(m) = \Delta^{(n)}(m) - f_n \Psi_n^{(\bar{s})}(m),$$

$$f_n := (\Delta^{(n)}, \Psi_n^{(\bar{s})})_N, \qquad \Delta^{(0)}(m) := F(m). \tag{14}$$

The signal is thus finally represented as

$$F(m) = f_0 \Psi_0^{(\bar{s})}(m) + f_1 \Psi_1^{(\bar{s})}(m) + \cdots + f_{N-1}\Psi_{N-1}^{(\bar{s})}(m) + \Delta^{(N)}(m), \tag{15}$$

where the coefficients $\{f_n\}_{n=0}^{N-1}$ will provide an alternative mode content vector for the signal. Note that there is no guarantee that the norm of the last difference vector in Eq. (15), $|\Delta^{(N)}(m)|$, will be zero. Both sampling analyses (13) and (15) will now be compared with the sampling analysis afforded by the Kravchuk basis in Eq. (12) and with the "true" mode coefficients of the field.

5. HARMONIC ANALYSIS IN THREE BASES

Assume that we have a setup whose continuous-output field $\bar{F}(x)$ can be subject to analysis and synthesis in the full basis of harmonic oscillator modes, $\Psi_n(x) \in \mathcal{L}^2(\Re)$, as

$$\bar{F}(x) = \sum_{n=0}^{\infty} \bar{F}_n \Psi_n(x), \quad \bar{F}_n = \int_{-\infty}^{\infty} \mathrm{d}x \Psi_n(x) \bar{F}(x), \quad n|_0^{\infty}, \tag{16}$$

yielding the infinite set of "true" mode coefficients, $\{\bar{F}_n\}_{n=0}^{\infty}$. The first N of these can now be compared with the mode coefficients of the Kravchuk analysis, $\{F_n^{\mathrm{K}}\}_{n=0}^{N-1}$ in Eq. (12), with the s-HG mode coefficients $\{F_n^{\mathrm{S}}\}_{n=0}^{N-1}$ in Eq. (13), and with the fair-play mode coefficients $\{f_n\}_{n=0}^{N-1}$ in Eq. (14). With these coefficients we shall then examine the fidelity of their synthesis to restore the original N-point signal.

For test function we consider a real and centered rectangle signal [$F(x)=1$ for $|x| \leq 5.5$, and 0 otherwise], sampled at the $N=31$ points $x_m = \bar{s}m$ for integer $m|_{-j}^{j}$ ($j=15$), with the corresponding optimal scale factor $\bar{s}=0.258253$ from the table of numbers, Eq. (11). We choose this sharp-edged signal for mode analysis because it presents a wide spectrum of modes; Gaussian-smooth test functions are often too compliant with expectations. In Fig. 6 we compare the "true" mode coefficients of the field, normalized by the ratio $\bar{F}_n/\bar{F}_0$, together with the corresponding Kravchuk mode coefficients $F_n^{\mathrm{K}}/F_0^{\mathrm{K}}$ so that both coincide at 1 for $n=0$; for odd n they are zero due to parity. In the insets of the figure, we show the true mode coefficients for n's well beyond $2j=N-1=30$; they exhibit a sinc-like decrease and a beat that reminds us of the Fourier series coefficients of the same rectangle function. This feature can be traced to the fact that the middle portion of large-n oscillator states approximates a cosine or a sine curve (for n even or odd) having n zeros in an interval that grows as $\sim n^{1/2}$ (cf. Fig. 5) and accounting for the visible lengthening of the beat periods. Finally, we insert the s-HG mode coefficients $F_n^{\mathrm{S}}/F_0^{\mathrm{S}}$ obtained from Eq. (13).

We note that (for $N=31$), the Kravchuk mode coefficients $\{F_n^{\mathrm{K}}\}_{n=0}^{30}$ match the true coefficients of the field up to $n \approx 7$ (and at $n=30$), that they have the same sign up to $n \approx 17$, and that they differ thereafter. On the other hand, the mode coefficients in the s-HG basis—$\{F_n^{\mathrm{S}}\}_{n=0}^{30}$ obtained from Eq. (13)—are manifestly unfit to approximate the true mode content of the rectangle function, since even its lowest modes do not follow the pattern of the main graph in Fig. 6.

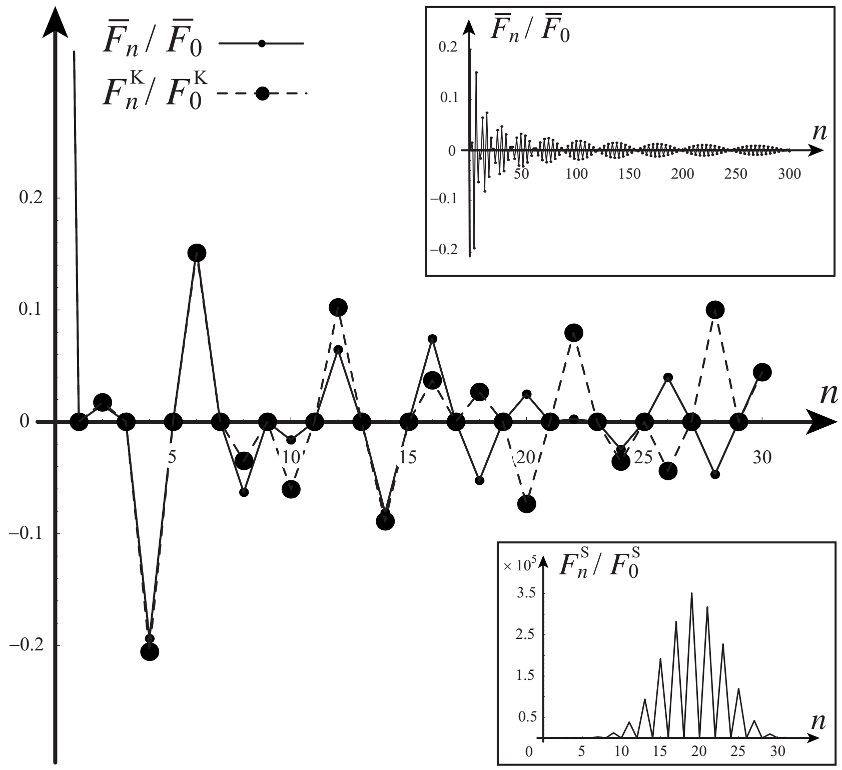

Fig. 6. True mode coefficients $\{\bar{F}_n/\bar{F}_0\}_{n=0}^{30}$, from Eq. (16) for $N=31$, of the rectangle signal that is nonzero for $m\in[-5,5]$, indicated by small dots and joined by solid lines for visibility. Superposed are the Kravchuk mode coefficients $\{F_n^K/F_0^K\}_{n=0}^{30}$ from Eq. (12), indicated by large dots joined by dotted lines. (Their common value 1 for $n=0$ is outside the graph.) Top inset, true mode coefficients up to $n=300$; bottom inset, sampled HG mode coefficients $\{F_n^S/F_0^S\}_{n=0}^{30}$ of the same data set from Eq. (13); notice the very large coefficients, $\approx 3.5\times 10^5$ for $n\approx 20$.

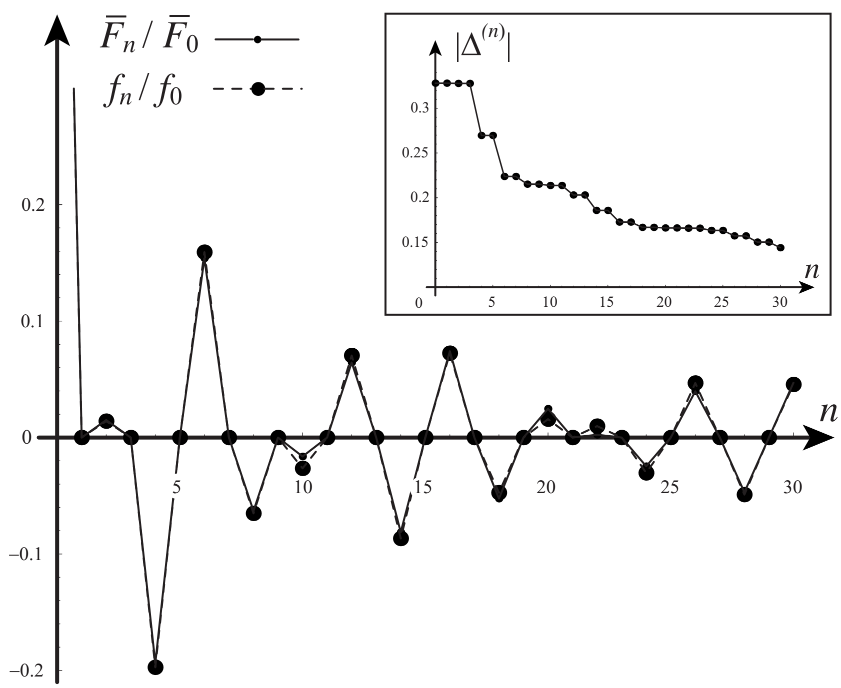

Fig. 7. True mode coefficients $\{\bar{F}_n/\bar{F}_0\}_{n=0}^{30}$ of the rectangle function from Eq. (16), as in Fig. 6, compared with the s-HG mode coefficients $\{f_n/f_0\}_{n=0}^{30}$ obtained as from Eq. (14). Inset, norms of the difference vectors $|\Delta^{(n)}|$ in Eq. (16).

In Fig. 7 is shown the result when the s-HG vectors are used to provide the mode coefficients $\{f_n\}_{n=0}^{30}$ from Eqs. (14) and (15) for the same rectangle function. There we see an almost perfect match with the true mode content, so we conclude that the s-HG basis can provide a very good approximation to the true modes of the continuous field. The only discernible differences in Fig. 7 occur at mode numbers $n=10$ and 20–26. Yet, because the basis of sampled HG's are not orthogonal, we confirm our suspicion that the norms of the difference vectors, $|\Delta^{(n)}|$ in Eq. (15), do not decrease to zero. An inset in the figure shows the difference between the original rectangle signal (scaled to have norm 1) and its full synthesis by s-HG functions, which ends with a difference norm of 0.1442. Therefore, Eq. (15) cannot reproduce the original signal at all its points.

The second part of our three mode analyses concerns the fidelity of their syntheses in restoring the signal through a sequence of approximations by sums over the modes $n \leqslant M$, truncated to $M+1 \leqslant N$ terms—and also, although the physical meaning is unclear, the behavior of the analytic continuation of the approximant functions for $m \in [-j,j]$. In Fig. 8 is shown the successive approximations to the rectangle function by the true, s-HG, and Kravchuk functions, for selected values of $M \leqslant N-1$. We note that the HG reconstruction by $\bar{F}_{N-1}(m)$ exhibits a Gibbs-like phenomenon at the discontinuities (as expected), both on the sample points and in their analytic interpolations; this persists, with little difference or improvement up to the highest $M=N-1$. Of course, discrete signals are discontinuous by nature, so "discontinuity" should be understood here as a "large difference between two adjoining signal points." Finally, Fig. 8 also shows the synthesized Kravchuk approximants to the signal values and their analytic continuation. For the highest M's the Kravchuk approximants display shorter oscillations inside the rectangle and quickly go to zero elsewhere, while the analytic continuations oscillate ever more strongly near the end points of the interval.

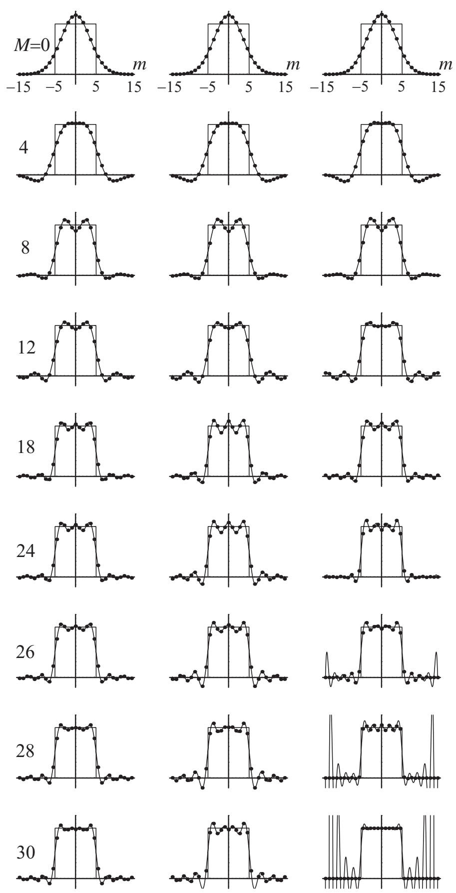

Fig. 8. Successive approximations to the finite rectangle signal on $N=31$ points ($j=15$) by truncated sums of modes $0 \leqslant n \leqslant M$ for $M=0$, 4, 8, 12, 18, 22, 24, 26, 28, and 30. Left column, the true modes $\{\bar{F}_n\}_{n=0}^{M}$ from Eq. (16) synthesized with HG functions; dots mark the values at the sensor points $m|_{-j}^{j}$. Middle column, the s-HG mode coefficients $\{f_n\}_{n=0}^{M}$ from Eq. (14), also synthesized with the continuous HG functions. Right column, the Kravchuk mode coefficients $\{F_n^{\mathrm{K}}\}_{n=0}^{M}$ synthesized with Kravchuk functions at the sensor points and their analytical continuation. The signal restoration is exact for $M+1=N=31$.

6. CONCLUSIONS

While Fourier integral analysis and its periodic and finite sampled versions are well understood and widely used in communication theory, harmonic analysis in terms of oscillator modes requires function bases that obey the oscillator dynamics and are related by an appropriate scale factor.

The first line of comparison between the Kravchuk and s-HG bases of $\mathcal{V}^N$ was dictated by mathematical preference for orthonormality and completeness. This straightforward approach to analyzing finite signals in their formant modes is well served by the Kravchuk functions, while it fails for the "almost-incomplete" s-HG functions. The latter seem to work best in the second comparison line, when only its mode content is sought and the requirement to restore the signal is dropped. At some cost in its fidelity in reproducing the true mode coefficients of the continuous field, only the Kravchuk basis achieves the exact restoration of the original signal.

For two-dimensional fields, sampled to form Cartesian-pixelated images, a straightforward generalization of the previous analysis and synthesis is the direct product of two one-dimensional ones, combined to form orthonormal bases of two Kravchuk or Laguerre–Kravchuk vectors [16,17]. Moreover, group theory also affords a distribution of sensor points on circles [18] that would seem fit to analyze beams with angular momentum. Finally, discrete- and finite-oscillator models can be set up using q special functions [19] that will sample the field with non-equally-spaced sensor points.

ACKNOWLEDGMENTS

I express my thanks to Tatiana Alieva (Departamento de Óptica, Universidad Complutense de Madrid) for suggesting this mode analysis problem and to Guillermo Krötzsch of the Instituto de Ciencias Físicas (ICF)-Universidad Nacional Autónoma de Mexico (UNAM) for essential aid with the figures. I also acknowledge the support of the Dirección General de Asuntos del Personal Académico (DGAPA)-UNAM project IN-105008 Optica Matemática.

REFERENCES

1. D. G. Luenberger, *Optimization by Vector Space Methods* (Wiley, 1969).
2. J.-B. Martens, "The Hermite transform—theory," IEEE Trans. Acoust., Speech, Signal Process. **38**, 1607–1618 (1990).
3. N. Tanguy, P. Vilbé, and L. C. Calvez, "Optimum choice of free parameter in orthonormal approximations," IEEE Trans. Autom. Control **40**, 1811–1813 (1995).
4. A. C. den Brinker and H. J. W. Belt, "Optimal free parameters in orthonormal approximations," IEEE Trans. Signal Process. **46**, 2081–2087 (1998).
5. A. C. den Brinker and B. E. Sarroukh, "Modulated Hermite series expansion and time-bandwidth product," Signal Process. **80**, 243–250 (2000).
6. T. Alieva and M. J. Bastiaans, "Mode analysis through the fractional transforms in optics," Opt. Lett. **24**, 1206–1208 (1999).
7. T. Alieva and K. B. Wolf, "Finite mode analysis through harmonic waveguides," J. Opt. Soc. Am. A **17**, 1482–1484 (2000).
8. N. M. Atakishiyev and K. B. Wolf, "Fractional Fourier–Kravchuk transform," J. Opt. Soc. Am. A **14**, 1467–1477 (1997).
9. N. M. Atakishiyev, L. E. Vicent, and K. B. Wolf, "Continuous vs. discrete fractional Fourier transforms," J. Comput. Appl. Math. **107**, 73–95 (1999).
10. N. M. Atakishiyev, G. S. Pogosyan, and K. B. Wolf, "Finite models of the oscillator," Phys. Part. Nucl. **36**, 521–555 (2005).
11. B. E. Sarroukh, "Signal analysis representation tools," Ph. D. thesis (Technische Universiteit Eindhoven, The Netherlands, 2001).
12. K. B. Wolf and G. Krötzsch, "Geometry and dynamics in the fractional discrete Fourier transform," J. Opt. Soc. Am. A **24**, 651–658 (2007).
13. L. C. Biedenharn and J. D. Louck, "Angular momentum in quantum mechanics," in *Encyclopedia of Mathematics and Its Applications*, G.-C. Rota, ed. (Addison-Wesley, 1981); Sec. 3.6.
14. M. Krawtchouk, "Sur une généralization des polinômes d'Hermite," C. R. Acad. Sci. Paris **189**, 620–622 (1929).
15. N. M. Atakishiyev, G. S. Pogosyan, and K. B. Wolf, "Contraction of the finite one-dimensional oscillator," Int. J. Mod. Phys. A **18**, 317–327 (2003).
16. N. M. Atakishiyev, G. S. Pogosyan, L. E. Vicent, and K. B. Wolf, "Finite two-dimensional oscillator. I: The Cartesian model," J. Phys. A **34**, 9381–9398 (2001).
17. K. B. Wolf and T. Alieva, "Rotation and gyration of finite two-dimensional modes," J. Opt. Soc. Am. A **25**, 365–370 (2008).
18. N. M. Atakishiyev, G. S. Pogosyan, L. E. Vicent, and K. B Wolf, "Finite two-dimensional oscillator. II: The radial model," J. Phys. A **34**, 9399–9415 (2001).
19. N. M. Atakishiyev, A. U. Klimyk, and K. B. Wolf, "Finite q-oscillator," J. Phys. A **37**, 5569–5587 (2004).